Hindawi
Advances in Materials Science and Engineering
Volume 2023, Article ID 3085478, 11 pages
https://doi.org/10.1155/2023/3085478

Research Article

Investigation on the Mechanical Properties of Powder Metallurgy-Manufactured AA7178/$ZrSiO_4$ Nanocomposites

R. Srinivasan,[1] S. Karunakaran,[2] M. Hariprabhu,[3] R. Arunbharathi,[4] S. Suresh,[5] S. Nanthakumar,[6] S. K. H. Ahammad,[7] S. Mayakannan,[8] and Mani Jayakumar [9]

[1]*Sri Krishna College of Technology, Coimbatore, Tamilnadu, India*
[2]*Department of Chemical Engineering, KPR Institute of Engineering and Technology, Coimbatore, Tamilnadu, India*
[3]*Department of Electrical and Electronics Engineering, M. Kumarasamy College of Engineering, Karur, Tamilnadu, India*
[4]*Department of Mechanical Engineering, Sri Krishna College of Engineering and Technology, Coimbatore, Tamilnadu, India*
[5]*Department of Chemistry, St. Martin's Engineering College, Secunderabad, Telangana, India*
[6]*Department of Mechanical Engineering, PSG Institute of Technology and Applied Research Neelambur, Coimbatore, Tamilnadu, India*
[7]*Department of Electronics and Communication Engineering, Koneru Lakshmaiah Education Foundation, Vijayawada 522302, India*
[8]*Department of Mechanical Engineering, Vidyaa Vikas College of Engineering and Technology, Tiruchengode, Namakkal, Tamilnadu, India*
[9]*Department of Chemical Engineering, Haramaya Institute of Technology, Haramaya University, P.B. No. 138, Dire Dawa, Ethiopia*

Correspondence should be addressed to Mani Jayakumar; drjayakumarmani@haramaya.edu.et

Received 13 January 2023; Revised 7 April 2023; Accepted 4 May 2023; Published 22 May 2023

Academic Editor: V. Vijayan

The versatility of metal matrix composites (MMCs) makes them a promising material for various industrial applications. The current study used a ball milling to mechanically AA7178 powder and strengthened with zirconium silicate ($ZrSiO_4$) nanoparticles. In addition, the AA7178 matrix was ball-milled to distribute the $ZrSiO_4$ nanoparticles throughout the material. The AA7178 reinforced with $ZrSiO_4$ nanoparticles was compacted and consolidated using two distinct powder metallurgy (PM) sequences: double pressing, double sintering, and hot pressing. In tests measuring microhardness, compression strength, and elongational break, the new nanocomposites surpassed the AA7178. The adequate interfacial bonding and even distribution of $ZrSiO_4$ nanoparticles throughout the AA7178 matrix were essential to the strengthening mechanism. With the use of hot pressing, the mechanical characteristics of the nanocomposites were enhanced. As reinforcement concentration increased beyond 2.5% by weight, mechanical properties drastically degraded due to $ZrSiO_4$ nanoparticles clumping and unequal distribution. Improved mechanical parts attain through the uniform distribution of $ZrSiO_4$ nanoparticles in the AA7178 and the maintenance of their mechanical properties.

1. Introduction

Due to naturally enhanced mechanical capabilities and exceptional weight, $ZrSiO_4$ nanoparticles have been the focus of research and development in the scientific and industrial communities over the past decade [1]. Applications in transportation and security, where the combination of lighter materials with improved mechanical qualities is desirable, show great promise for the use of $ZrSiO_4$ nanoparticles as reinforcing material for the fabrication of MMC [2]. Close connections developed between the matrix and the scattered $ZrSiO_4$ nanoparticles, which helped to fine-tune the grain and boost the mechanical characteristics of the materials. The mechanisms of grain refining, load transfer,

and Orowan looping provide the basis of the reinforcement contributions [3, 4]. $ZrSiO_4$ nanoparticles are often researched as reinforcing materials due to their higher efficiency and simplicity of manufacture. However, $ZrSiO_4$ nanoparticles offer better mechanical characteristics (from 60 to 160 GPa) and high elastic modulus (1.9 TPa) [5].

The latest review by the authors [6] indicates that several studies discuss using powder methods to reinforce aluminum or aluminum alloys. However, effective nanoaluminum alloy composites with state-of-the-art properties continue to be hampered by various obstacles brought on by the features of $ZrSiO_4$ nanoparticles [7]. The most urgent issues to be addressed include clustering, minimal wettability of $ZrSiO_4$ nanoparticles with aluminum, and the development of numerous distinct phases at 450°C, such as aluminum carbide (Al_4C_3) or aluminum oxides [8–10]. Aluminum-$ZrSiO_4$ nanoparticles interfacial bond strength, $ZrSiO_4$ aspect ratio, and nano $ZrSiO_4$ quality all play a vital role in the mechanical characteristics of $ZrSiO_4$-reinforced aluminum alloys [11–13].

Many different chemical pretreatments have been applied to the $ZrSiO_4$ nanoparticles, and conditions have been used in the $ZrSiO_4$ nanoparticle powder combination (like nanoparticles or graphite) to enhance the original shape and surface qualities of metal powders [14, 15]. Ball milling is frequently used, but because of the lengthy milling process substantial damage to $ZrSiO_4$ nanoparticles, the Nano $ZrSiO_4$/Al composite's mechanical characteristics are typically subpar [16, 17]. Composite aluminum alloy reinforced with $ZrSiO_4$ nanoparticles can be made using a wide variety of powder consolidation techniques, such as cold pressing, hot pressing, hot extrusion, and spark plasma sintering (SPS) [18].

The research reports the fabrication of AA7075-based hybrid composites using TiO_2 and fly ash as reinforcements via stir casting and hot forging. The mechanical behavior of the composites was studied through compression tests, showing increased compressive strength with higher weight fractions of TiO_2. The coefficient of thermal expansion decreased with the addition of TiO_2 and fly ash, while a slight decrease in thermal conductivity was observed compared to AA7075 [19].

The study reports on the development of A357 alloy composite reinforced with dual size SiC particles by stir casting. Different weight fractions of dual size SiC particles were investigated for their influence on mechanical properties and wear resistance of A357 composites. The composites showed improvement in hardness, yield, and tensile strength compared to A357 alloy, with 4 wt. % of fine and 2 wt. % of large SiC particles displaying the highest tensile strength and 4 wt. % of large and 2 wt. % of fine SiC particles exhibiting high hardness and wear resistance [20].

Aluminum alloy composites with graphene nanoplates were produced by ball milling and stir casting. The addition of graphene nanoplates reduced grain size and increased the strength of the composites. T6 heat treatment improved the strength of the composites, but at higher graphene content, agglomerates on grain boundaries facilitated crack growth [21].

Aluminum hybrid composites were produced using powder metallurgy with varying weight fractions of graphene and fixed CNT content. Wear tests were conducted with varying applied load, and worn surface analysis was done using SEM. Increasing graphene content increased bulk hardness and reduced wear rate due to the formation of a lubricating layer [22]. Aluminum hybrid composites were developed using powder metallurgy technique with Si_3N_4 and CNT as reinforcements. Scanning electron microscope studies showed uniform dispersion of both reinforcements. Microhardness increased with CNT content, electrical conductivity decreased, and coefficient of friction decreased due to the lubricating nature of CNTs [22, 23].

This research successfully produced AA7178 reinforced with $ZrSiO_4$ nanoparticles using milling, mechanical alloying, and two distinct compaction and sintering processes. The proposed manufacturing processes use commercial technologies that could enable mass production of high-value AA7178/$ZrSiO_4$ nanocomposites for use in demanding lightweight constructions, including armored assault vehicles. The goal was to minimize structural failure of the $ZrSiO_4$ nanoparticles while achieving a homogeneous dispersion of the nanoparticles in the metal matrix using powder technology approaches that could eventually lead to commercial mass production. Al7075 nanocomposites with varying B4C contents were produced using powder metallurgy technique. Microstructure, grain size, and wear behavior were analyzed. Dry sliding wear test was conducted using Taguchi L9 approach, and the most influential parameter on wear volume was found to be the B4C nanoparticle content.

2. Methods and Materials

The AA7178 created through mechanical alloying, and its nominal composition is 2% copper, 2.7% magnesium, 6.8% zinc, and aluminum balance. The Sigma/Aldrich firm obtained all the materials mentioned previously. The AA7178 mix matrix was created in a high-energy, vertically agitated ball mill for three hours at 500 revolutions per minute to avoid oxidation during production. Powder agglomeration was avoided by adding a small amount of ethanol to the mixture. Stearic acid was added to the mix at a 1 wt. % to ensure uniformity throughout the manufacturing process [24, 25]. The researcher used a 10 : 1 ball-to-powder ratio in our mechanical alloying technique involving stainless-steel balls.

Ball milling was also employed to create the nanocomposite material. The previously milled AA7178 powder was combined with various amounts of $ZrSiO_4$ nanoparticles (1.5, 2.5, 3.5, 4.5, 5.5, and 6.5 wt. %) in a planetary ball mill with the same milling conditions. To avoid damaging the $ZrSiO_4$ nanoparticles, the milling speed was reduced to 250 rpm, and the milling time was extended to 60 minutes.

"A stainless-steel cylinder mold with an internal radius of 9 mm was used to perform uniaxial compression on milled powder combinations of AA7178 and $ZrSiO_4$ nanoparticles. Graphene oxide was used as an additive to

reduce the effects of friction. Hot-pressing (HP) and double pressing and sintering techniques (DPST) were used for compaction. The powder used to create the AA7178 for this investigation is shown in Figure 1(a)."

After being heated and compacted under 250 MPa of pressure for 10 minutes at a specific temperature of 400°C, the milled composite powder mixes were presintered in a low vacuum furnace for 60 minutes at 520°C. Green compacts were lightly sprayed with a graphite spray to reduce resistance to the mold before being pressed for a second time. After 10 minutes at 400°C and 550 MPa, the second hot compaction was completed. After preheating to 590°C, the green compacts were sintered for 120 minutes in a low vacuum.

For the HP process, hot pressing was done for 60 minutes at 400 MPa under 550°C on mixtures of milled composite powders. The green compacts were heated to 590°C for 120 minutes in a low vacuum environment. Milled AA7178 were hot-pressed, and sintered AA7178 were both processed for this study.

Both sintered composite samples and milled composite powders have their crystal structures evaluated using X-ray diffraction (XRD). During this sintering process, a TA Instruments DSC 25 differential scanning calorimeter was used to determine the phase transition from RT to 600°C at 15°C/min. Microstructural characterization and phase distribution in sintered composite samples were assessed using SEM [26, 27].

Sintered composite samples were subjected to mechanical testing on a Vickers microhardness analyzer with a 100 g load and a dwell time of 20 seconds [28]. At least five readings were averaged to arrive at the final microhardness value using a strain rate of 0.01 s^{-1}, which is common for materials with lower modulus. The researcher performed quasistatic compression tests, with each sample tested three times to achieve repeatable and dependable results. The compressive stress-strain characteristics were determined by averaging the data from the three tests. The dimensions of the samples used for ASTM E9 solid compressive testing were calculated. Small samples are commonly used for compressive testing since compliant metals, which are often used as thin plates to transmit vertical load to the surfaces, are typically employed [29]. In the compression test, each sample was 20 mm long and 16 mm in diameter ($L/D = 1.25$). Scanning electron microscopy (SEM) was employed to analyze the fractured surfaces of specimen pieces taken from the crushed materials [30, 31].

3. Results and Discussions

3.1. Sintered Composite and Milled Composite Structural Property. The flake-shaped morphology of the AA7178 powder created after the ball-milling process is considered favorable for incorporating $ZrSiO_4$ nanoparticles into the matrix [32, 33]. Ball-milled AA7178/$ZrSiO_4$ nanoparticles powder mixtures are shown in SEM. There were no $ZrSiO_4$ nanoparticle aggregates to be seen, indicating that they had been evenly distributed and integrated into the AA7178 powders. Although most of the $ZrSiO_4$ nanoparticles look fragmented and smaller than the original ones, their estimated length is still sufficient, demonstrating that ball milling did not cause damage.

Figure 2 shows the X-Ray Diffraction pattern for the milled AA7178, and the milled AA7178-$ZrSiO_4$ nanocomposites. The $ZrSiO_4$ nanoparticles peak at $2\theta = 34°$, identical to the graphite *C* height, is readily observed [34–36]. The peak's exceptional sharpness indicates that the two-dimensional Graphene layer providing the tubular pattern of the zirconia has nearly perfect crystallinity. A further indicator of the $ZrSiO_4$ nanoparticles' excellent purity is that the *C* curve was not filtered toward the highest values of 2θ (greater than 34°). At $2\theta = 46°$, also known as the graphite peak, and at $2\theta = 78°$, also known as the graphite peak, are peaks of noticeably lesser intensity [37, 38]. These peaks are not crisp. Hence the crystallinity of the different $ZrSiO_4$ nanoparticles can differ. The enlargement of this peak may indicate that other graphitized carbon types are present [39–41].

Both milled AA7178 samples show aluminum diffraction peaks. There are also a few peaks that are associated with copper and magnesium. Magnesium peaks vanish after 2 hours of $ZrSiO_4$ nanoparticles milling on the AA7178, leaving only copper peaks to be seen. Both the intensity and the width of these peaks are waning. This outcome implies that mechanical alloying was used successfully to produce AA7178. Once the $ZrSiO_4$ nanoparticles are fine-tuned, the remaining *C* peaks vanish, suggesting that few of the *C* content has been liquefied into the aluminum to generate a solid state. For the AA7178-2.5 wt. % after milling, a differential scanning calorimeter was performed. This assumption was tested by a process involving 100% $ZrSiO_4$ nanoparticles.

In Figure 3, the DSC curve is displayed. This low-temperature first peak is associated with the evaporation and subsequent release of humidity from ethanol. A small exothermic peak between 410 and 440°C was observed for the AA7178-$ZrSiO_4$ nanoparticles powder mixture. Al_4C_3 formation may be related to this peak. During sintering, the metastable Al-C solid solution breaks down, forming Al_4C_3 [42].

In contrast, the XRD patterns of milled AA7178-$ZrSiO_4$ nanoparticles did not show any broadening of the aluminum peaks compared to milled AA7178. This shows that aluminum's structure has not absorbed significant carbon material. The aluminum's lattice parameter and crystallite size remained constant throughout all examined situations, indicating that the metal contains negligible amounts of carbon [43, 44]. Milled and sintered AA7178-$ZrSiO_4$ nanoparticle samples exhibited XRD structures devoid of pronounced Al_4C_3 peaks. This confirms that the $ZrSiO_4$ nanoparticles utilized in this analysis are steady when interacting with aluminum and do not break into aluminum carbide [45]. The XRD results show that the $ZrSiO_4$ nanoparticles are the most excellent possible quality and contain no silicon oxide or imperfections in the carbon [46].

Specimens of milled and sintered AA7178-$ZrSiO_4$ nanoparticles, manufactured using the HP process, with (a) 4.5% and (b) 2.5% $ZrSiO_4$ nanoparticles compositions, are

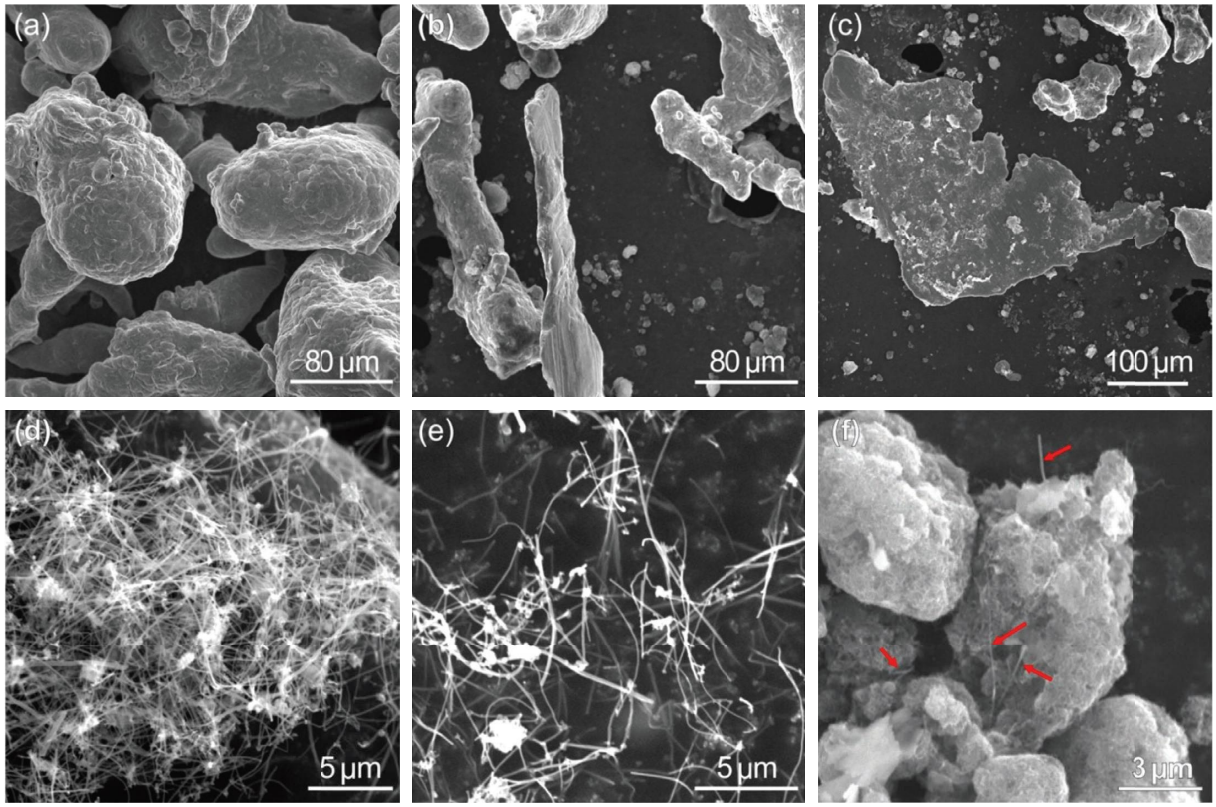

FIGURE 1: Scanning electron microscopic image of (a) initial AA7178 utilized, (b and c) AA7178 next to ball milling, (d and e) $ZrSiO_4$ nanoparticles utilized, (f) AA7178 and $ZrSiO_4$ nanoparticles next to ball milling.

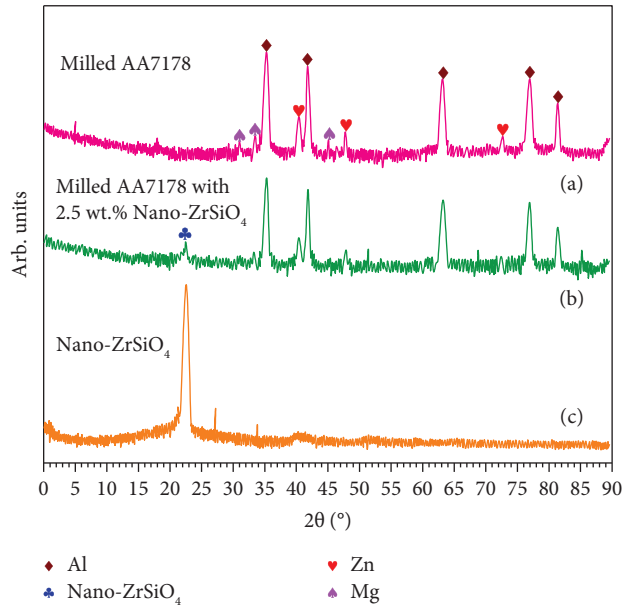

FIGURE 2: X-ray diffraction pattern of (a) AA7178, (b) 2.5% $ZrSiO_4$ nanoparticles powder mixtures, and (c) AA7178 reinforced with $ZrSiO_4$ nanoparticles.

shown as XRD patterns in Figure 4. Sintered AA7178 in its purest form is displayed in Figure 4(c). While sintering eliminated the oxide peak, the intermetallic phase Al_2O was still present in all sintered specimens (AA7178 and the composite), regardless of the $ZrSiO_4$ nanoparticles amount. The microstructure progression of intermetallic stages in

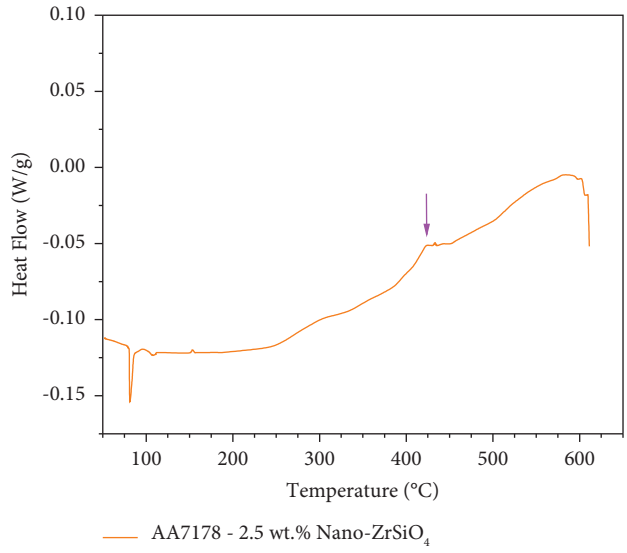

Figure 3: DSC curvature for the composite AA7178-2.5 wt. % $ZrSiO_4$ nanoparticles specimen.

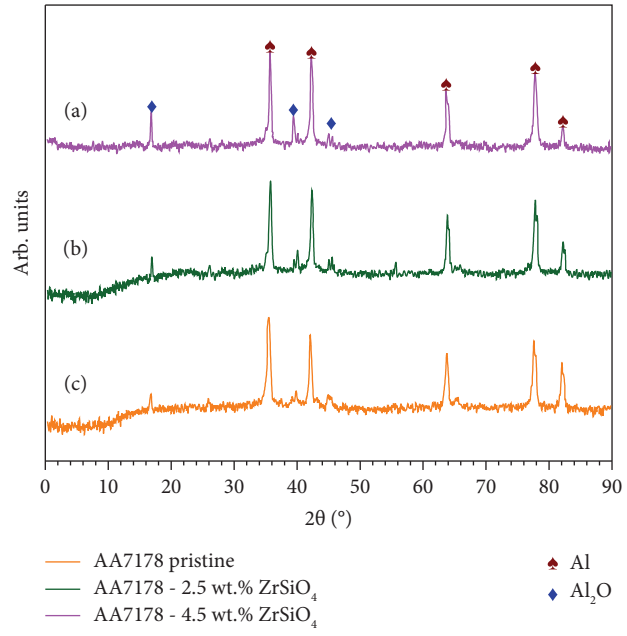

Figure 4: X-ray diffraction pattern of sintered and milled (a) AA7178-4.5 wt. % $ZrSiO_4$ nanoparticles and (b) AA7178-2.5 wt. % $ZrSiO_4$ nanoparticles (HP technique) and the (c) pristine AA7178.

AA7178 is significantly influenced by zirconia, as evidenced by the considerable changes in the intensity of these peaks with increasing $ZrSiO_4$ nanoparticles content.

Each composite material XRD pattern lacked the characteristic $ZrSiO_4$ nanoparticles *C* peak (Figures 4(a) and 4(b)). Due to low concentration of $ZrSiO_4$ nanoparticles on the surface of the specimen under analysis and the small scattering distance among carbon and metal atoms.

Microstructures of the AA7178-2.5% $ZrSiO_4$ nanoparticles composite produced by the two compaction techniques are shown in Figure 5. Both approaches consolidate the metal particles well. All methods can identify the intermetallic Al_2O phase, which can be easily identified by the lines and is found in both the grain borders and the interior regions of the grains. HP techniques appear to favor the formation of Al_2O intermetallic phases in the nanocomposite's microstructure. The DPSD compaction method preserves the flake shape of the initial AA7178 powders. HP causes grain strengthening.

Furthermore, the nanocomposite made using HP techniques exhibits subgrains. For instance, a few subgrains are indicated by red-dashed lines. This result provided support for the hypothesis that the hot-pressing technique led to grain strengthening via two distinct methodologies: (i) demolition of the flake morphologies of the ball-milling utilized, resulting in particle size drop of the first grains generated by the AA7178 and (ii) formation of the particle within these grains. This dynamic recovery and recrystallization cause high levels of plastic strain and heat, which are stamps of HP.

In contrast, the first grains for AA7178 powders are only revealed using the DPDS technique. Given the high oxygen content, these regions seem to belong to Al_2O. These oxides developed in the open air at the hot compaction phase of both production processes. The metallographic processing of this sample likely caused any porosity in this oxide by fracturing such brittle stages, leading to the formation of pores [47]. The argon atmosphere employed in the DPDS process causes varied shapes of the oxides. When HP is given to Al-$ZrSiO_4$ nanoparticles composites in a neutral atmosphere, the amorphous Al_2O_3 transforms into coarse, lump-shaped crystalline Al_2O_3 at matrix grain boundaries. The AA7178 grains must contain the oxide due to the high oxygen content. Additionally, due to the reaction of $ZrSiO_4$ nanoparticles with aluminum to generate brittle aluminum carbides, the oxide is present in the AA7178 grains [48].

3.2. Mechanical Properties. Figure 6(a) depicts the stress-strain relationship under compression for DPDS-created AA7178 nanocomposites with various $ZrSiO_4$ nanoparticles. Adding $ZrSiO_4$ nanoparticles, even at a low concentration of 2.5% by weight, enhances the nanocomposite's mechanical characteristics. Figures 6(a) and 6(b) indicate that for the 4.5% $ZrSiO_4$ nanoparticles with AA7178 nanocomposite, the results improve with increasing $ZrSiO_4$ nanoparticles content. Below the percentage mentioned above, mechanical properties begin to deteriorate noticeably. The observed findings explain the weak interface bonding among the AA7178 and the $ZrSiO_4$ nanoparticles, caused by the silicon oxide clustering and unequal distribution in the AA7178 matrix.

$ZrSiO_4$ nanoparticles have been shown to play an essential role in the compression behavior and modulus of AA7178 nanocomposites. When the concentration of $ZrSiO_4$ nanoparticles in AA7178 is increased, it causes a significant increase in the yield stress, indicating that the

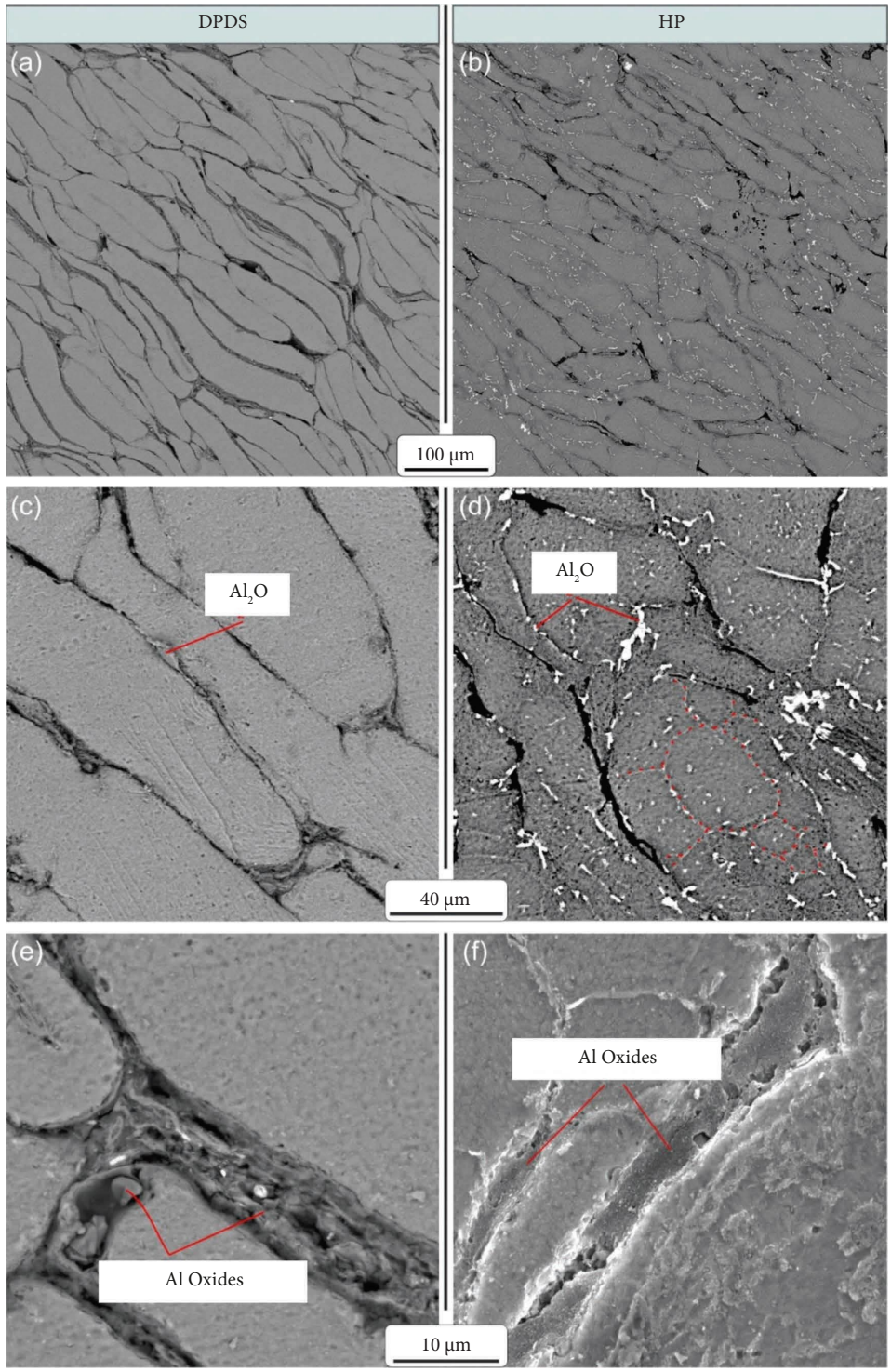

Figure 5: Microstructure of AA7178-2.5 weight. % $ZrSiO_4$ nanoparticles generated via double pressing double sintering (a, c, e), hot pressing (b, d, f).

nanoparticles strengthen the composite. This is because the nanoparticles create barriers to dislocation motion, which causes an increase in the yield stress. In addition, the $ZrSiO_4$ nanoparticles also contribute to the increased modulus of the composite. This is because the nanoparticles are stiffer than the aluminum matrix, and their incorporation into the composite results in a stiffer overall structure. The increased modulus also means that the composite is more resistant to deformation.

However, as the concentration of $ZrSiO_4$ nanoparticles is further increased to 2.5%, the compression behavior of the composite starts to deteriorate. This is because the nanoparticles become clustered, resulting in the formation of large clusters that can cause cracks in the composite. The

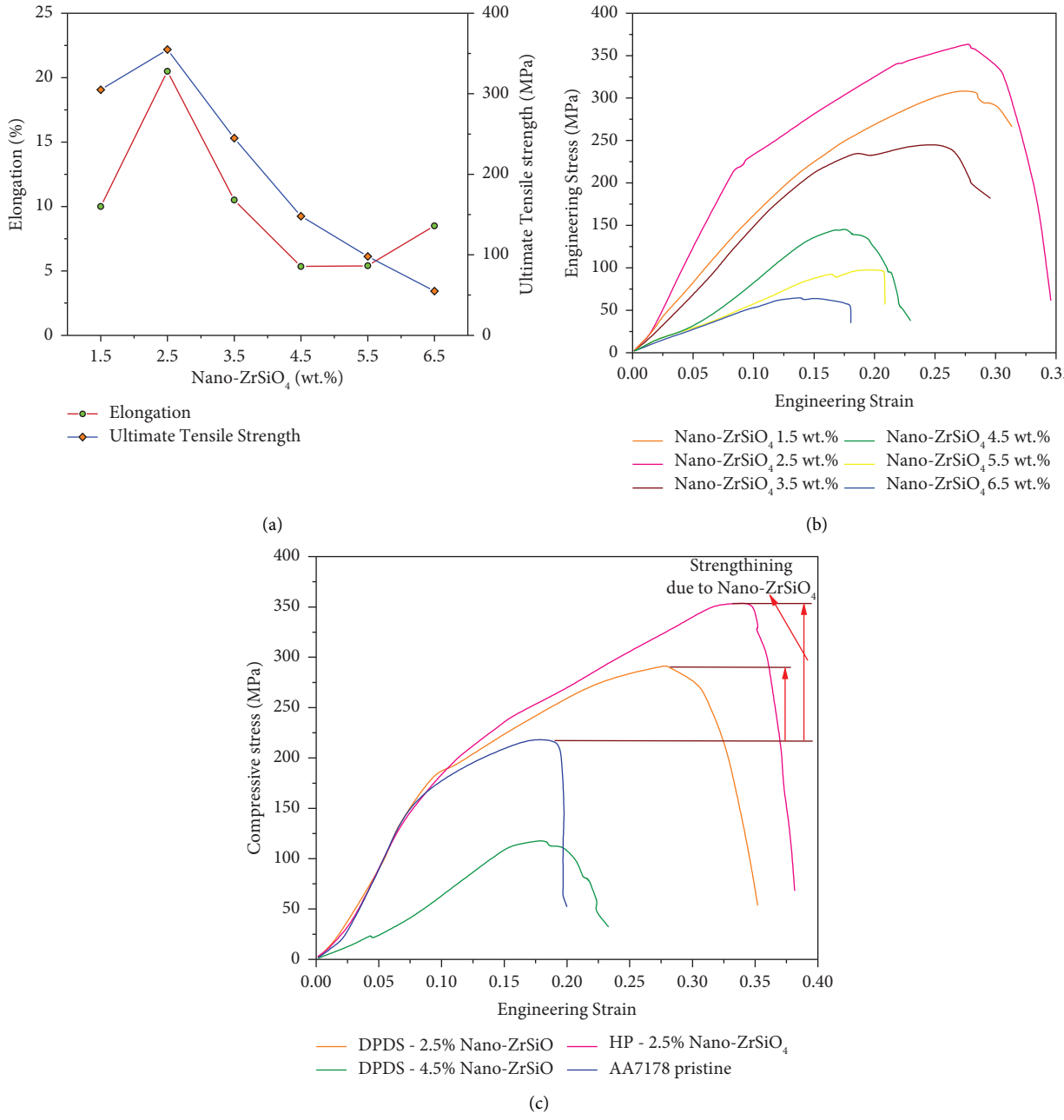

Figure 6: (a) Ultimate tensile strength and elongation values. (b) Compressive stress-strain curvature with various reinforcement of $ZrSiO_4$ nanoparticles with DPDS technique and (c) compressive stress-strain curvature of the AA7178 at various reinforcement with different PM techniques.

cracks act as stress concentrators and reduce the strength of the composite, leading to a decrease in the yield stress and modulus. Therefore, the concentration of nanoparticles should be carefully controlled to achieve the optimal balance between strength and toughness.

Figure 6(b) displays stress and strain curvature and representative images of tested samples for AA7178 and numerous AA7178-$ZrSiO_4$ nanocomposites made under varying conditions. For comparison, the researcher also provides flawless AA7178 (Figure 6(b)). The AA7178-2.5% $ZrSiO_4$ nanoparticles composite produced by the DPDS or HP techniques has ultimate strength and considerably higher yield than pure AA7178. Fracture elongation was also greatly improved from 0.13 for AA7178 to 0.19 for the double pressing double sintering technique and 0.21 for the hot-pressing approach. The improved flexibility of the AA7178 matrix can be accredited to the uniform dispersal of $ZrSiO_4$ nanoparticles throughout the matrix [49].

Young's modulus and other mechanical parameters of the nanocomposite are improved more by the HP compaction method than by the DPDS approach. The matrix material has been refined, leading to a denser composite.

Table 1: Comparison of microhardness for various conditions.

Constituents	Pristine AA7178	Double pressing double sintering		Hot pressing 2.5 wt. % $ZrSiO_4$ nanoparticles
		2.5 wt. % $ZrSiO_4$ nanoparticles	4.5 wt. % $ZrSiO_4$ nanoparticles	
Microhardness $HV_{0.1}$	58	64	51	72

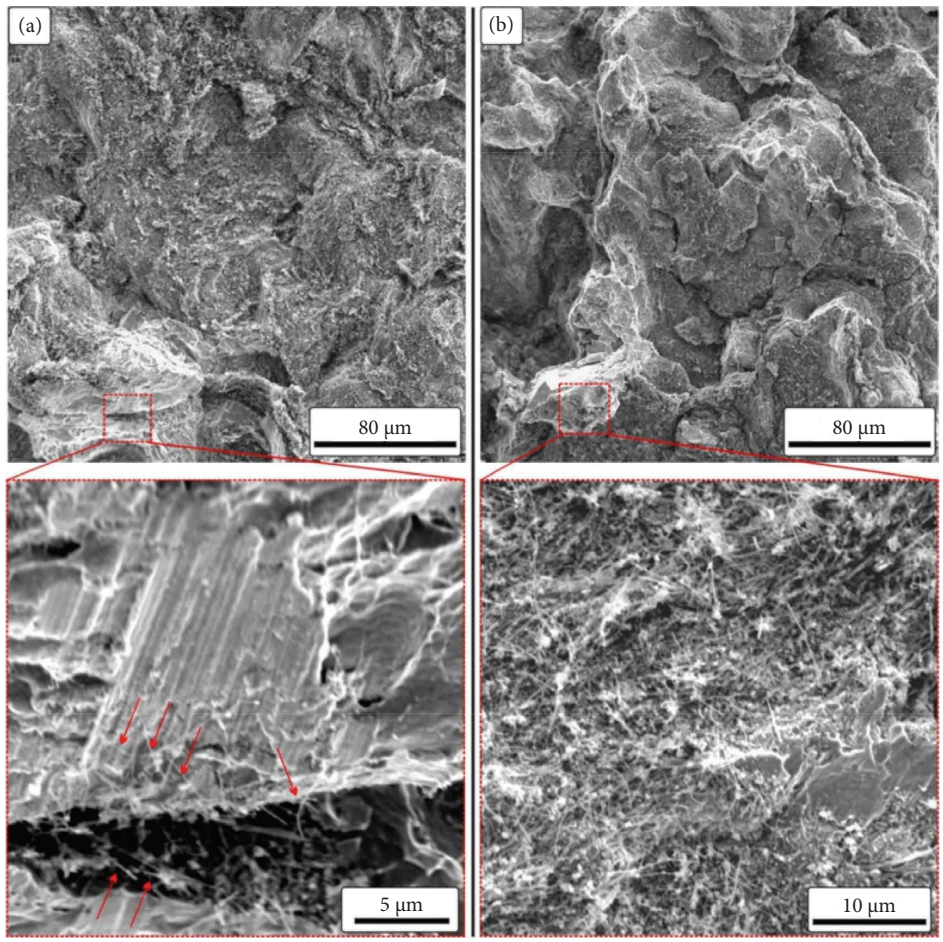

Figure 7: Scanning electron microscope of fracture surfaces: (a) AA7178-2.5% $ZrSiO_4$ nanoparticles and (b) AA7178-4.5% $ZrSiO_4$ nanoparticles generated through DPDS technique.

Compared to the HP method, which yielded composites with a density of 2.65 g/cm^3 (equal to 98%), the DPDS method yielded composites with a thickness of 2.6 g/cm^3 (equivalent to 93.5% of the theoretical value). When comparing AA7178-2.5 wt. % $ZrSiO_4$ nanoparticles produced by DPDS and HP, the strength-ductility effectiveness (compressive strength × elongation) was calculated to be 5.25 GPa for DPDS and 8.17 GPa for HP, showing that the balance among highest strength and elasticity was effectively attained in the case of HP.

The AA7178 matrix and $ZrSiO_4$ nanoparticles may strengthen the resultant nanocomposites through various mechanisms, including grain boundary reinforcement, grain strengthening, stress transfer from AA7178 to $ZrSiO_4$ nanoparticles, and Orowan looping. $ZrSiO_4$ nanoparticles alone reveal essential reinforcing when the aluminum grains are more significant than the strengthening, and the ZrSiO4 nanoparticles are predominantly positioned on the grain restrictions, as is the case here.

Utilizing the increased mechanical properties of the nanotubes requires a successful load transfer from the AA7178 matrix to the $ZrSiO_4$ nanoparticles. Mechanical parameters correlate highly with $ZrSiO_4$-AA7178 interfacial bonding, $ZrSiO_4$ nanoparticles structural integrity, and uniform nanotube dispersion in the metal matrix. Reinforcement of the composites may also result from a favorable mechanism, the contact of dislocations with the nanotubes. A fractographic study of compressed samples was carried out to verify the load transmission.

The mechanical compressive testing findings demonstrate that the composites made with AA7178-2.5 wt. % $ZrSiO_4$ nanoparticles are more complex than pure AA7178.

This is supported by the composite materials' microhardness ratings (Table 1). The AA7178-4.5 wt. % $ZrSiO_4$ nanoparticles nanocomposite is much less mechanically robust, as evidenced by microhardness measurements. The samples passed microhardness testing with flying colors, demonstrating efficient load transmission because of the lack of cracking.

Figure 7 shows the SEM images of the cracked surfaces of AA7178-$ZrSiO_4$ nanocomposites with 2.5 wt. % and 4.5 wt. % $ZrSiO_4$ nanoparticles content, respectively. Load transmission efficiency at the $ZrSiO_4$/matrix contact was demonstrated by $ZrSiO_4$ nanoparticle pull-outs (arrows) on the AA7178 fracture surface. The pull-outs evident during tensile testing provide insight into the load transferring at the $ZrSiO_4$ nanoparticles/matrix interaction and the disposition of $ZrSiO_4$ nanoparticles during the fracturing behavior of the sample. Some places were subjected to shear and tension, even if the overall application of stress was just compressive. Extensive pull-outs indicate a strong connection between the matrix and the $ZrSiO_4$ nanoparticles, enhancing strengthening effects. These exceptionally long pull-outs prove that the silicon oxide was not significantly reduced in length during milling. It is important to note that the distribution of pull-out $ZrSiO_4$ nanoparticles in the broken surfaces of the samples under study was correlated with their existence.

Cracks in an AA7178-4.5 wt. % $ZrSiO_4$ nanoparticles nanocomposite reveal clusters of $ZrSiO_4$ nanoparticles and inhomogeneous distribution in the matrix (Figure 7(b)). Poor mechanical qualities result from aggregate formation, which weakens the interfacial bond among the $ZrSiO_4$ nanoparticles and AA7178 composites. According to the results of other researchers [50, 51], the percentage of $ZrSiO_4$ nanoparticles employed in the reinforcement can be used to estimate the maximum content of the integrated reinforcement, with a lower portion resulting in more distribution of $ZrSiO_4$ nanoparticles in the matrix.

4. Conclusions

An AA7178 composite reinforcing with $ZrSiO_4$ nanoparticles was successfully created employing a mechanical alloy process and milling process, succeeded by two compacting and sintering processes. The produced nanocomposites' mechanical characteristics and corresponding microstructural morphologies were investigated and correlated. Insights like these can be gleaned from the data:

(1) Both compaction methods led to the development of a composite material with improved mechanical properties when compared to pure AA7178 alloy. However, the high-pressure (HP) method resulted in a composite with denser microstructure and smaller grain size, which led to even better mechanical properties. Despite experiencing significant splintering, the structural integration of the $ZrSiO_4$ nanoparticles remained intact. It is likely that the fracturing facilitated the efficient transmission of loads from the aluminum matrix to the $ZrSiO_4$ nanoparticles.

(2) The study demonstrated a direct correlation between the mechanical strength of the composite and the amount of $ZrSiO_4$ nanoparticles added to the matrix, up to a certain point. However, adding more than 2.5 wt. % $ZrSiO_4$ nanoparticles caused a significant reduction in the mechanical properties of the composite due to the clustering of the nanoparticles.

(3) The AA7178-2.5wt. % $ZrSiO_4$ nanocomposite, when produced using the DPDS method, exhibited a compressive strength of 372 MPa, while the same nanocomposite manufactured through the HP approach displayed a higher strength of 445 MPa. However, both methods resulted in the development of nanocomposites with sufficient strength-ductility efficiency, as evidenced by their elongation values of 19% and 21%, respectively.

Data Availability

The data supporting the current study are available from the corresponding author upon request.

Conflicts of Interest

The authors declare that they have no conflicts of interest.

Acknowledgments

The authors would like to sincerely thank those techniques that have contributed to this research.

References

[1] F. Gillani, M. Z. Khan, and O. R. Shah, "Sensitivity analysis of reinforced aluminum based metal matrix composites," *Materials*, vol. 15, pp. 4225–4312, 2022.

[2] H. Abdizadeh, M. Ashuri, P. T. Moghadam, A. Nouribahadory, and H. R. Baharvandi, "Improvement in physical and mechanical properties of aluminum/zircon composites fabricated by powder metallurgy method," *Materials & Design*, vol. 32, no. 8–9, pp. 4417–4423, 2011.

[3] N. Bharat and P. S. C. Bose, "Optimization of tribological behaviour of TiO2nanoparticles reinforced AA7178 alloy matrix using ANN and Taguchi's methodology," *Surface Topography: Metrology and Properties*, vol. 10, no. 2, Article ID 025032, 2022.

[4] T. A. Amibo, S. M. Beyan, M. Mustefa, V. P. Sundramurthy, and A. B. Bayu, "Development of nanocomposite based antimicrobial cotton fabrics impregnated by nano SiO2 loaded AgNPs derived from eragrostis teff straw," *Materials Research Innovations*, vol. 26, no. 7, pp. 405–414, 2021.

[5] R. Saravanan, C. Gnanavel, S. Rajesh, T. Kamatchi, S. Ajith Arul Daniel, and D. K. Nagarathi, "Synthesis of Zinc oxide and CNT in AA7178 aluminium alloy composite impression on characteristics," *Materials Today: Proceedings*, vol. 62, pp. 1973–1976, 2022.

[6] J. R. Xavier, "Improvement of mechanical and anticorrosion coating properties in conducting polymer poly(propyl methacrylate) embedded with silane functionalized silica nanoparticles," *Silicon*, vol. 13, no. 10, pp. 3291–3305, 2021.

[7] A. H. S. Shatha, M. Rajaa Abduljabbar, A. N. Abood, and H. A. Abdulhadi, "Evaluation the effect of shot peening time

on static torsional strength of AA7178-T6," *Journal of Engineering and Applied Sciences*, vol. 13, no. 12, pp. 4476–4481, 2018.

[8] M. Banerjee, T. N. Verma, and P. Nashine, "Experimental and numerical analysis of extrusion process for AA 7178 alloy with varying process parameters," *Materials Today: Proceedings*, vol. 5, no. 2, pp. 6839–6847, 2018.

[9] C. Vidal, V. Infante, and P. Vilaça, "Metallographic characterization of friction stir channels," *Materials Science Forum*, vol. 730, pp. 817–822, 2012.

[10] C. Vidal, V. Infante, and P. Vilaça, "Mechanical characterization of friction stir channels under internal pressure and in-plane bending," *Key Engineering Materials*, vol. 488, pp. 105–108, 2011.

[11] V. Mohanavel and M. Ravichandran, "Optimization of parameters to improve the properties of AA7178/Si3N4 composites employing Taguchi approach," *Silicon*, vol. 14, no. 4, pp. 1381–1394, 2022.

[12] P. Chattoraj, P. Prabhakar, V. Koti et al., S. P. Kumar, Optimization on tribological behaviour of aa7178/nano titanium diboride hybrid composites employing Taguchi techniques," *Journal of Nanomaterials*, vol. 2022, Article ID 1619923, 8 pages, 2022.

[13] S. D. Kumar, M. Ravichandran, A. Jeevika, B. Stalin, C. Kailasanathan, and A. Karthick, "Effect of ZrB2 on microstructural, mechanical and corrosion behaviour of aluminium (AA7178) alloy matrix composite prepared by the stir casting route," *Ceramics International*, vol. 47, no. 9, pp. 12951–12962, 2021.

[14] G. S. V. S. Kumar, A. Kumar, S. Rajesh, R. B. R. Chekuri, and V. P. Sundaramurthy, "Experimental and thermal investigation with optimization on friction stir welding of nylon 6A using Taguchi and microstructural analysis," *Advances in Mechanical Engineering*, vol. 13, no. 10, Article ID 168781402110507, 2021.

[15] V. Mohanavel, K. Yoganandam, V. N. Kumar, A. Chandrashekar, and S. Prasath, "Evaluation of tribological behaviour of AA7178/Gr composites using Taguchi optimization technique," *Materials Today: Proceedings*, vol. 33, pp. 4691–4695, 2020.

[16] V. Mohanavel, "Mechanical and microstructural characterization of AA7178-TiB2 composites," *Materials Testing*, vol. 62, no. 2, pp. 146–150, 2020.

[17] S. D. Kumar, M. Ravichandran, and 'Synthesis, "Synthesis, characterization and Wire electric erosion behaviour of AA7178-10 wt.% ZrB2 composite," *Silicon*, vol. 10, no. 6, pp. 2653–2662, 2018.

[18] S. D. Kumar and M. Ravichandran, "Synthesis, properties and EDM behavior of 10 wt.-% ZrB2 reinforced AA7178 matrix composites," *Materials Testing*, vol. 60, no. 9, pp. 877–884, 2018.

[19] K. Shivananda Murthy, D. P. Girish, R. Keshavamurthy, T. Varol, and P. G. Koppad, "Mechanical and thermal properties of AA7075/TiO2/Fly ash hybrid composites obtained by hot forging," *Progress in Natural Science: Materials International*, vol. 27, no. 4, pp. 474–481, 2017.

[20] A. Lakshmikanthan, S. Bontha, M. Krishna, P. G. Koppad, and T. Ramprabhu, "Microstructure, mechanical and wear properties of the A357 composites reinforced with dual sized SiC particles," *Journal of Alloys and Compounds*, vol. 786, pp. 570–580, 2019.

[21] G. A. Kumar, J. Satheesh, K. V Murthy, H. M. Mallikarjuna, N. Puneeth, and P. G. Koppad, "Optimization of Wear Properties of B4C Nanoparticle-Reinforced Al7075 Nanocomposites Using Taguchi Approach," *Journal of The Institution of Engineers (India): Series D*, vol. 104, pp. 1–12, 2022.

[22] M. Alipour, R. Keshavamurthy, P. G. Koppad, A. Shakiba, and N. C. Reddy, "Investigation of microstructure and mechanical properties of cast Al–10Zn–3.5 Mg–2.5 Cu nanocomposite reinforced with graphene nano sheets produced by ultrasonic assisted stir casting," *International Journal of Metalcasting*, vol. 17, no. 2, pp. 935–946, 2022.

[23] M. H. R. Naik, L. H. Manjunath, V. Koti, A. Lakshmikanthan, P. G. Koppad, and S. P. Kumaran, "Al/Graphene/CNT hybrid composites: hardness and sliding wear studies," *FME Transactions*, vol. 49, no. 2, pp. 414–421, 2021.

[24] K. Shanmuganandam, S. Thanikaikarasan, T. Ahamad, S. Ali, and V. P. Sundramurthy, "Structure, surface nature, thermal stability, and biomass gasification process of NiO/SiO2 and NiO-Pr2O3/SiO2 nanocomposites obtained through facile deposition precipitation method," *Journal of Nanomaterials*, vol. 2022, Article ID 1479808, 9 pages, 2022.

[25] D. R. Belichko, T. E. Konstantinova, G. K. Volkova et al., E. Popov, Effects of YSZ ceramics doping with silica and alumina on its structure and properties," *Materials Chemistry and Physics*, vol. 287, Article ID 126237, 2022.

[26] A. P. Pasupulla, P. Amornphimoltham, T. T. Halabo, H. Abebe, and M. M. Ramakrishna, "Microstructure and characterization of Al 6082 alloy with addition of ZrSiO4and TiC reinforcements," *AIP Conference Proceedings*, vol. 2473, 2022.

[27] L. Wang, B. Ma, X. Ren et al., Z. Jiang, Phase-engineering strategy of ZrO2 for enhancing the mechanical properties of porous cordierite ceramics," *Materials Today Communications*, vol. 30, Article ID 103032, 2022.

[28] H. Zhang, "Preparation of porous ceramic building decoration materials by foaming method and research on nanomechanical properties," *International Journal of Analytical Chemistry*, vol. 2022, Article ID 8339503, 7 pages, 2022.

[29] C. G. Soubelet and M. P. Albano, "Differences in microstructure and mechanical properties between Y-TZP and AL2O3-doped Y-TZP/bioglass ceramics," *International Journal of Applied Ceramic Technology*, vol. 18, no. 6, pp. 2237–2249, 2021.

[30] M. A. Violini, M. F. Hernández, M. Gauna, G. Suarez, M. S. Conconi, and N. M. Rendtorff, "Low (and negative) thermal expansion Al2TiO5 materials and Al2TiO5 - 3Al2O3.2SiO2 - zrTiO4 composite materials. Processing, initial zircon proportion effect, and properties," *Ceramics International*, vol. 44, no. 17, pp. 21470–21477, 2018.

[31] M. T. Souza, G. M. Peñarrieta-Juanito, B. Henriques, F. S. Silva, A. P. Novaes de Oliveira, and J. C. M. Souza, "Lithium-zirconium silicate glass-ceramics for restorative dentistry: physicochemical analysis and biological response in contact with human osteoblast," *Materialia*, vol. 2, pp. 37–45, 2018.

[32] M. F. Zawrah, R. S. Farag, and M. H. Kohail, "Improvement of physical and mechanical properties of geopolymer through addition of zircon," *Materials Chemistry and Physics*, vol. 217, pp. 90–97, 2018.

[33] V. Ramesha, T. B. Prasad, V. Nayak, and V. L. Neelakantha, "A study on mechanical properties of Al-17Si metal matrix composites," *IOP Conference Series: Materials Science and Engineering*, vol. 376, Article ID 012100, 2018.

[34] N. Liao, D. Jia, Z. Yang, Y. Zhou, and Y. Li, "Enhanced mechanical properties, thermal shock resistance and oxidation resistance of Si2BC3N ceramics with Zr-Al addition,"

Materials Science and Engineering: A, vol. 725, pp. 364–374, 2018.

[35] P. Li, "Tribological properties and microstructures of Al2O3-TiC-TiB2 reinforced composites," *Science and Engineering of Composite Materials*, vol. 24, no. 5, pp. 715–720, 2017.

[36] M. Sharifitabar, M. Kashefi, and S. Khorshahian, "Effect of friction stir processing pass sequence on properties of Mg-ZrSiO4-Al2O3 surface hybrid micro/nano-composites," *Materials & Design*, vol. 108, pp. 1–7, 2016.

[37] N. M. Rendtorff, S. Gómez, M. R. Gauna, M. S. Conconi, G. Suarez, and E. F. Aglietti, "Dense mullite-zirconia-zirconium titanate ceramic composites by reaction sintering," *Ceramics International*, vol. 42, no. 1, pp. 1563–1572, 2016.

[38] T. S. Kumar, R. Subramanian, S. Shalini, and P. C. Angelo, "Microstructure, mechanical properties and corrosion behaviour of Al–Si–Mg alloy matrix/zircon and alumina hybrid composite," *Forschung im Ingenieurwesen*, vol. 79, no. 3–4, pp. 123–130, 2015.

[39] S. K. Thandalam, S. Ramanathan, and S. Sundarrajan, "Synthesis, microstructural and mechanical properties of ex situ zircon particles (ZrSiO4) reinforced Metal Matrix Composites (MMCs): a review," *Journal of Materials Research and Technology*, vol. 4, no. 3, pp. 333–347, 2015.

[40] M. Feng, C. Jiang, M. Chen, S. Zhu, and F. Wang, "A general strategy towards improving the strength and thermal shock resistance of glass-ceramics through microstructure regulation," *Journal of Materials Science & Technology*, vol. 120, pp. 139–149, 2022.

[41] F. Stergioudi, A. Prospathopoulos, A. Farazas, E. C. Tsirogiannis, and N. Michailidis, "Mechanical properties of AA2024 aluminum/MWCNTs nanocomposites produced using different powder metallurgy methods," *Metals*, vol. 12, pp. 1315–1318, 2022.

[42] F. Lin, F. Jia, M. Ren et al., "Microstructure, mechanical and thermal properties of ultrafine-grained Al2024–TiC-GNPs nanocomposite," *Materials Science and Engineering: A*, vol. 841, Article ID 142855, 2022.

[43] P. Ashwath, M. A. Xavior, R. Rajendran, A. D. L. Batako, P. Jeyapandiarajan, and J. Joel, "Microwave-assisted T6 heat treating of aluminium alloy-Al2O3 nanocomposites," *MRS Communications*, vol. 12, no. 2, pp. 245–249, 2022.

[44] S. Rokkala, V. K. Ambati, D. K. Mellam, R. Nethala, and B. V. S. A. Kumar, "Predicting impact strength and hardness of aluminium & tungsten carbide nano-composite synthesized by PM," *Materials Today: Proceedings*, vol. 67, pp. 342–350, 2022.

[45] Y. Sun, A. Li, Y. Hu, X. Wang, and M. Liu, "Simultaneously enhanced strength-plasticity of graphene/metal nanocomposites via interfacial microstructure regulation," *International Journal of Plasticity*, vol. 148, Article ID 103143, 2022.

[46] V. Shrivastava, G. Kumar Gupta, H. Jain, D. Mangal, P. Singh, and I. B. Singh, "Novel synthesis approach of making efficient nanocomposite via powder metallurgy route: study of microstructure and mechanical properties," *Manufacturing Letters*, vol. 31, pp. 36–39, 2022.

[47] M. Çelebi, O. Güler, A. Çanakçı, and H. Çuvalcı, "The effect of nanoparticle content on the microstructure and mechanical properties of ZA27-Al2O3-Gr hybrid nanocomposites produced by powder metallurgy," *Journal of Composite Materials*, vol. 55, no. 24, pp. 3395–3408, 2021.

[48] P. Shrivastava, S. N. Alam, T. Maity, and K. Biswas, "Effect of graphite nanoplatelets on spark plasma sintered and conventionally sintered aluminum-based nanocomposites developed by powder metallurgy," *Materials Science-Poland*, vol. 39, no. 3, pp. 346–370, 2021.

[49] M. R. Mattli, P. R. Matli, A. Khan et al., "Study of microstructural and mechanical properties of al/sic/tio2 hybrid nanocomposites developed by microwave sintering," *Crystals*, vol. 11, no. 9, p. 1078, 2021.

[50] V. Gholipour, M. Shamanian, A. Ashrafi, and A. Maleki, "Development of aluminium-nanoclay composite by using powder metallurgy and hot extrusion process," *Metals and Materials International*, vol. 27, no. 9, pp. 3681–3694, 2021.

[51] G. Huang, J. Wu, W. Hou et al., F. Meng, A novel two-step method to prepare fine-grained SiC/Al-Mg-Sc-Zr nanocomposite: processing, microstructure and mechanical properties," *Materials Science and Engineering: A*, vol. 823, Article ID 141764, 2021.